Supra-molecular assembly of aromatic proton sponges to direct the crystallization of extra-large pore zeotypes

Raquel Martínez-Franco,[a] Junliang Sun,[b] German Sastre,[a] Yifeng Yun,[b] Xiaodong Zou,[b] Manuel Moliner,[*a] Avelino Corma[*a]

[a] *Instituto de Tecnología Química (UPV-CSIC), Universidad Politécnica de Valencia, Consejo Superior de Investigaciones Científicas, Valencia, 46022, Spain*

[b] *Berzelii Centre EXSELENT on Porous Materials and Inorganic and Structural Chemistry, Department of Materials and Environmental Chemistry, Stockholm University, SE-106 91 Stockholm, Sweden.*

**Corresponding author: E-mail address: acorma@itq.upv.es, mmoliner@itq.upv.es*

Abstract

The combination of different experimental techniques, such as solid ^{13}C and ^{1}H MAS NMR spectroscopy, fluorescence spectroscopy, and powder X-ray diffraction, together with theoretical calculations allows the determination of the unique structure directing role of the bulky aromatic proton sponge 1,8-bis(dimethylamino)naphthalene (DMAN) towards the extra-large pore ITQ-51 zeolite through supra-molecular assemblies of those organic molecules.

Keywords:

Zeolite, proton sponge, supra-molecular, organic structure directing agent, catalysis

1.- Introduction

Bulky and rigid organic structure directing agents (OSDAs) can be useful for the preparation of zeolites with large void volumes, and especially for the synthesis of extra-large pore zeolites.[1] Using large and rigid OSDAs different extra-large pore zeolites presenting mono-directional 14-ring channels,[2] multidimensional extra-large channels,[3] and even mesoporous zeolites [4] have been synthesized. In these cases, the zeolite crystallization occurs through the interaction of single organic molecular units and the inorganic sources present in the synthesis gel. Bulky and rigid OSDAs must be soluble in the synthesis media (usually aqueous media), present high hydrothermal stability, and more importantly, have strong non-bonded interactions with the host inorganic matrix during nucleation-crystallization processes.[5] However, when the C/N ratio is increased above a certain value (C/N>14), some solubility problems of these bulky OSDAs in aqueous media can appear, precluding their structure directing capacity.[1]

Several years ago, a new organic structure directing concept based on supramolecular assemblies was introduced in the preparation of zeolites, and the pure silica small pore large volume A zeolite (LTA) was synthesized breaking the paradigm that this zeolite could only be synthesized with high Al contents.[6] In this case, the bulky OSDA required to template the large LTA cavity and to allow minimization of framework negative charges, was achieved by the supramolecular self-assembling of two organic molecules presenting an aromatic ring, forming stable and soluble bulky dimers through π-π type interactions.[6] Later, similar supramolecular self-aggregation through π-π type interactions of aromatic molecules, such as benzylpyrrolidine, has also been described for the crystallization of the large pore AlPO-5 zeotype.[7]

Very recently, we have introduced a new type of aromatic OSDAs, i.e. an aromatic proton sponge (1,8-bis(dimethylamino)naphthalene [DMAN], see Figure 1), for the synthesis of the extra-large pore ITQ-51 zeotype, whose structure presents 16-ring channels.[8] DMAN is a commercially available bulky aromatic diamine with the amine groups in close proximity, providing high basicity (pKa>12.1) by the repulsion of the close electronic lone pairs.[9] This high basicity would favor their protonation in the synthesis media, allowing organic-inorganic interactions during the nucleation-crystallization processes.

We will show here a combination of experimental and computational techniques in order to evaluate the structure directing roles of these aromatic molecules, including their ability to be protonated and their self-aggregation as dimers in the synthesis gel and in the final as-

prepared solid. The proton sponge dimers will allow the stabilization of the 16-ring extra-large pores of the ITQ-51 zeolite.

2.- Experimental and computational details

2.1.- Synthesis

The synthesis procedure of ITQ-51 can be found in ref [8]. Aqueous solutions of DMAN were prepared by adding equimolecular amounts of the corresponding proton sponge and phosphoric acid. The ionic complex of DMAN with orthophosphoric acid was prepared by mixing 217.7 mg of H_3PO_4 (85%wt, Sigma-Aldrich), 257.2 mg of proton sponge (99%wt, Sigma-Aldrich), and 615.4 mg of water, and the resultant solution was liofilized to remove the solvent.

2.2.- Characterization

The solid-state NMR spectra were recorded at room temperature on a Bruker AV 400 spectrometer MAS. ^{13}C MAS NMR cross-polarization (CP) spectrum was recorded at a sample spinning rate of 5 kHz. ^{1}H MAS NMR spectrum was achieved with a spinning rate of 10 kHz at 400 MHz with a $\pi/2$ pulse length of 5 μs. ^{13}C and ^{1}H NMR chemical shifts was referenced to adamantine and TMS, respectively.

Steady-state photoluminescence measurements were recorded in a Photon Technology International (PTI) 220B spectrofluorimeter having a Xe arc lamp light excitation and Czerny-Turner monochromator, coupled to a photomultiplier. The solid samples were pressed between two windows Suprasil quartz cuvettes with a path length of 0.01 mm and placed at a 45° angle to both the excitation and emission monochromators. All measurements were carried out at room temperature.

2.3.- Refinement against powder XRD data

The structure model was refined by Rietveld refinement using TOPAS with soft restraints for T-O bond distances and rigid body restraints for the organic structure directing agents (OSDAs). The framework positions were fully occupied. There is one unique OSDA in the unit cell, with occupancy of 0.5. All the atoms were refined with isotropically and the atomic displacement parameters were restrained to be equal for similar atoms. The refinement of the ITQ-51 model was converged with R_F = 0.0281 and R_{wp} = 0.0667. The refinement detail is given in Table S1.

2.4.- Computational methods

Several energetic contributions are widely acknowledged to be at play such as electrostatic (long range) and van der Waals (short range) zeo-OSDA. A fundamental idea behind this approach is the fact that the location of the OSDA molecule is mainly dictated by short range van der Waals forces between the OSDA and the zeolite framework, being the oxygen atoms of the zeolite the most important in the interaction with the OSDA due to their large size and anionic character.

In order to estimate the OSDA location within the micropore void we use the following strategy: (i) one molecule of OSDA is located in the micropore of ITQ-51 and the minimum energy position is found through a simulated annealing type procedure with repeated cycles of molecular dynamics runs followed by energy minimization; (ii) the unit cell of ITQ-51 is filled with different loadings of each particular OSDA and the optimum loading is calculated as that which minimizes the total energy; (iii) once the optimum loading is found, we use minimization algorithms for the full system. Then, we calculate the final contributions to the energy of the subsystems as shown in equations (1)-(3).

$$E_{initial} = E_{frame} + E_{OSDA-OSDA} + E_{OSDA} \quad (1)$$

$$E_{final} = E_{frame'} + E_{frame'-OSDA'} + E_{OSDA'-OSDA'} + E_{OSDA'} \quad (2)$$

A full electrostatic model has been considered with OSDA molecules containing +1 charge. Due to the fact that the positions of the counteranions are unknown, the compensating charge has been uniformly distributed across the framework atoms in order to have a neutral unit cell.

And so, it is expected that the energy difference between the final and initial states is due to the SDA incorporation which should be a negative, hence stabilising, interaction. Some of the above terms will be positive, such as the energy difference regarding framework energy ($E_{frame'} - E_{frame}$) and OSDA energy ($E_{OSDA'} - E_{OSDA}$), and hence each of the individual moities experiences an energy increase in the synthesis process. However, the interaction between the zeolite framework and the SDA molecules ($E_{frame'-OSDA'}$) should be negative enough so as to compensate the previous energetic increase.

Combining equations (2)-(1), we obtain the final expression below which shows quantitatively whether the synthesis is more or less feasible with the corresponding OSDA molecule. The more negative the value, the more favorable the synthesis.

$$\Delta E_{synthesis} = \Delta E_{frame} + E_{frame'-OSDA'} + \Delta E_{OSDA-OSDA} + \Delta E_{OSDA} \quad (3)$$

The calculations in steps (i), (ii) and (iii) have been performed using lattice energy minimization techniques [10] and the GULP code,[11] employing a direct summation of the short range interactions with a cut off distance of 12 Å. The RFO (rational functional optimizer) technique was used as the cell minimization scheme with a convergence criterion of a gradient norm below 0.001 eV/Å. To account for the effect of the OSDA in the system, the forcefield by Kiselev et al. [12] has been used for the intermolecular OSDA–zeolite and OSDA–OSDA interactions. For the AlPO system, a force field developed in a previous study was employed.[13]

For a more in depth study of the interactions between the OSDA molecules, a full electron quantum approach based on new functionals containing dispersion terms has been used in order to get a more accurate picture of the intermolecular interactions and their role in the total OSDA-OSDA energy obtained. The functionals CAM-B3LYP [14] and LCWPBE [15] including dispersion have been used. In all cases the accurate TZVP basis set [16] has been employed, and the results have been checked against basis set convergence by also using the further improved QZVP basis set. The Gaussian09 software package was used for the optimization of the OSDA molecules using the DFT approach outlined above.

The calculated unit cell parameters are: a = 23.61 Å, b = 16.25 Å, c = 4.95 Å, α = 90.0°, β = 90.9°, γ = 90.0°. The calculated stacking shows a relative rotation of the two SDA molecules of 155°, observing a tilt of 82° between the plane of the aromatic rings and the c (vertical) axis. This tilt is 74° in the experimental case. The combination of two opposite forces balanced could explain the slight discrepancies between the calculated and the experimental OSDA orientations. In this sense, attractive OSDA-framework interactions would drive the geometry towards a 90° tilt angle, whilst short range repulsions due to the limited pore diameter lead to a larger tilt angle. It is suggested that the forcefield employed does not contain the appropriate balance between attractive and repulsive forces. Nevertheless, an overall reasonable correspondence of the calculated OSDA location has been found with loading and location similar to the experimentally observed (see Table S2).

3.- Results

In a previous work, we have demonstrated by elemental analysis and solid ^{13}C MAS NMR (see spectrum of the as-prepared ITQ-51 in Figure S1) that the proton sponge DMAN remains intact within ITQ-51 crystals after the crystallization process.[8] However, despite the high proton affinity of DMAN molecules to form stable ionic species containing intramolecular $[N\ldots H\ldots N]^+$ hydrogen bonding,[9,17] the protonated nature of the occluded DMAN molecules within as-

prepared ITQ-51 was not described. To properly analyze whether DMAN molecules are protonated or not, as-prepared ITQ-51 was characterized by solid ^{1}H MAS NMR spectroscopy. As seen in Figure 2c, two main peaks are observed, corresponding to hydrogen bonds bound to the aliphatic and aromatic carbons, which are centered at ~2 and ~6.8 ppm, respectively. In addition to those large peaks, a small peak appears at 18.5 ppm. Interestingly, similar chemical shifts (~17-18 ppm) have been described in the literature for the acidic proton shielded by the amino groups on different DMAN complexes with inorganic and organic acids.[17,18] The solid ^{1}H MAS NMR spectrum of commercially available DMAN only shows the two large peaks corresponding to protons bounded to the aliphatic and aromatic carbons (see Figure 2a), but no signal at ~18.5 ppm is observed. However, if an ionic complex of DMAN is prepared with orthophosphoric acid (see experimental section for details) to force the protonated DMAN to form, the ^{1}H MAS NMR spectrum clearly shows the small band at 18.5 ppm (see Figure 2b), corresponding to the acidic proton between the amino groups, confirming that the DMAN is in a protonated form in the as-prepared ITQ-51.

Once the protonated nature of DMAN molecules in the as-prepared ITQ-51 has been confirmed, the next step was to understand the directing roles of the aromatic proton sponge molecules during the zeolite crystallization process. As described above, the supramolecular chemistry has been rarely described in the structure direction of crystalline microporous materials, being through π-π type interactions of aromatic molecules the only examples reported.[6,7] However, if the chemical structure of DMAN molecule is considered, this proton sponge molecule shows the suitable size, rigidity, thermal stability, and hydrophobicity (aromatic naphthalene group), to be a potential candidate to form bulky dimers by supramolecular self-assembled OSDAs.

It was described during the synthesis of LTA that when self-assembling through π-π type interactions of aromatic molecules occurs, the fluorescence spectrum shows an intense shift of the emission band towards higher wavelengths by the strong interaction of the aromatic rings.[6] Having that in mind, we have prepared two aqueous solutions of DMAN at different concentrations, 5.10^{-4} M and 3 M, in order to study the fluorescence emission spectra of the diluted and concentrated solutions. The idea behind is that DMAN molecules would remain as monomers in highly diluted conditions while dimerization may occur under concentrated conditions. It is important to note that this DMAN concentration is the same as it was required in the preparative gel for the synthesis of ITQ-51. Since the UV-Vis spectrum of DMAN in aqueous solution shows a band centered at 285 nm (see Figure S2), the photoluminescence

study of both DMAN aqueous solutions is performed at the excitation wavelengths of 270, 285, and 300 nm. As it can be observed in Figure 3, both diluted and concentrated DMAN solutions present similar fluorescence emission spectra with a main fluorescence band centered at 475 nm. This result clearly indicates that self-interactions of DMAN molecules through π-π type interactions of aromatic molecules does not occur either in the diluted or concentrated solutions of DMAN and, therefore, it can be expected that dimers of DMAN molecules by π-π stacking will not take place during the synthesis of ITQ-51. Indeed, the fluorescence emission spectrum of the as-prepared ITQ-51 solid shows a shift of the fluorescence band towards a lower wavelength (~415 nm, see Figure 3), which could be attributed to a particular interaction of DMAN molecules in the confined space of the ITQ-51. Nevertheless, it can be asserted that neither in the synthesis gel nor in the final solid there is self-aggregation of DMAN molecules through π-π type interactions.

However, when both aqueous solutions of DMAN were studied by liquid ^{1}H NMR spectroscopy, intense chemical shifts can be observed for the hydrogen bound to the aliphatic and aromatic carbons, which depend on the concentration of DMAN (see Figure S3). The diluted DMAN solution shows peaks ranging from 7.9 to 7.6 ppm for the protons associated to the aromatic carbons and a peak centered at 3 ppm for the protons associated to aliphatic carbons (see Figure S3a). On the other hand, the concentrated DMAN solution presents the signals at 6.8-6.3 and 1.9 ppm, for the protons associated to the aromatic carbons and aliphatic carbons, respectively (see Figure S3b). These changes on the chemical shifts of more than 1 ppm in the liquid ^{1}H NMR spectra depending on the DMAN concentration would be associated to some self-interactions of DMAN molecules under concentrations similar to those used during the zeolite synthesis. Interestingly, the ^{1}H MAS NMR spectrum of the as-prepared ITQ-51 shows two broad peaks centered at 6.9 and 2.4 ppm (see Figure S3c), which resembles to the ^{1}H NMR spectrum of the concentrated DMAN solution. Particular confined issues of DMAN molecules within ITQ-51 structure could be the reason for the slightly different chemical shifts. Thus we could conclude from the ^{1}H NMR spectroscopy that a self-interaction of DMAN molecules may occur in the synthesis gel and in the final as-prepared ITQ-51 solid, but it cannot be unequivocally ascertain from the characterization results obtained so far.

To confirm or reject the formation of DMAN dimers, the structure model of the as-prepared ITQ-51 material has been developed using powder X-ray diffraction (PXRD) data. The structure model was refined by Rietveld refinement using TOPAS [19] with soft restraints for T-O bond distances and rigid body restraints for the OSDAs. The framework positions were fully occupied.

There are two OSDAs in one unit cell. All the atoms were refined isotropically and the atomic displacement parameters were restrained to be equal for similar atoms. The refinement of the ITQ-51 model converged to R_F = 0.0281 and R_{wp} = 0.0667. The refinement details are given in Figure 4 and Table S1. From the structure solution, it is observed that the OSDAs are located in the middle of the 16-ring channels with a rotation angle of 74° from the channel axis (Figure 5a), and form stacking OSDA-dimers (see Figure 5a and 5b).

A computational study has also been performed to further support the dimer formation (see experimental for details). In the optimized geometry of ITQ-51-OSDA (Figure S4a), it can be observed that the OSDA molecules are not perpendicular to the channel axis. Since the OSDA molecule is wider (9.2 Å) than the channel width (7.7 Å), the OSDA has to rotate (Figure S4b). This deviation from an ideal angle of 90° seeks to maximize the OSDA-framework attraction and also maximize the OSDA-OSDA interaction.

As described in the crystallographic structure model, the OSDA molecules adopt a stacking inside the zeolite which is not very different from that calculated in the gas phase, in spite of the fact that the pore size/shape represents a constraint for the optimization of the OSDA-dimer (see details in experimental and Table S2). Calculations at the level of first principles using DFT indicate a stabilization energy in gas phase of 4.1 kJ/mol-of-dimer. The present OSDA-dimer interactions are mainly driven by electrostatic and van der Waals interactions (see experimental and Table S3). Regarding the geometries of the OSDA-dimers in the zeolite framework, Figure 6 shows in detail that the bulky methyl groups are in opposite sides of the neighbor OSDA, with the aromatic rings parallel to each other. The OSDA-OSDA distance in the optimized ITQ51-OSDA system is 4.3 Å.

Conclusions

We have demonstrated by experimental and computational techniques the unique self-assembling role of the aromatic proton sponges in the synthesis of the extra-large pore ITQ-51 zeolite. In this sense, the design of new OSDAs allowing the control of their supramolecular chemistry can provide an efficient tool to direct the synthesis of new microporous materials, especially those presenting extra-large pore structures.

Acknowledgements

This work has been supported by the Spanish Government through Consolider Ingenio 2010-Multicat, the “Severo Ochoa Programme” (SEV 2012-0267), MAT2012-37160; UPV through PAID-06-11 (n.1952); the Swedish Research Council (VR) and the Swedish Governmental

Agency for Innovation Systems (VINNOVA). Manuel Moliner also acknowledges to “Subprograma Ramon y Cajal” for the contract RYC-2011-08972. German Sastre thanks SGAI-CSIC and ASIC-UPV for computational facilities.

Figure 1: Proton sponge 1,8-bis(dimethylamino)naphtalene [DMAN].

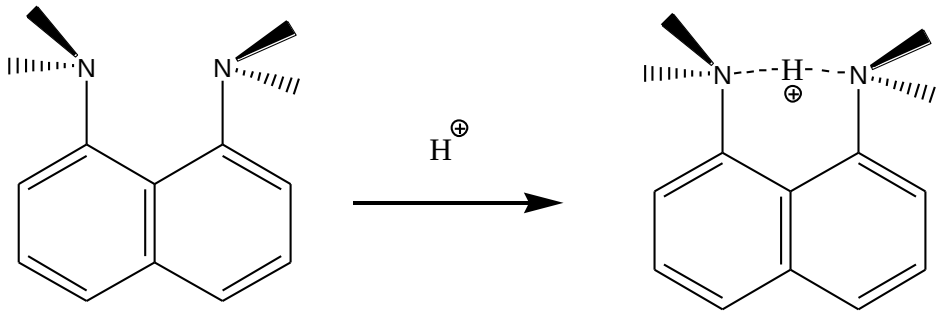

Figure 2: Solid ^{1}H MAS NMR spectra of DMAN (a), of the complex of DMAN with orthophosphoric acid (b), and as-prepared ITQ-51 molecular sieve (c).

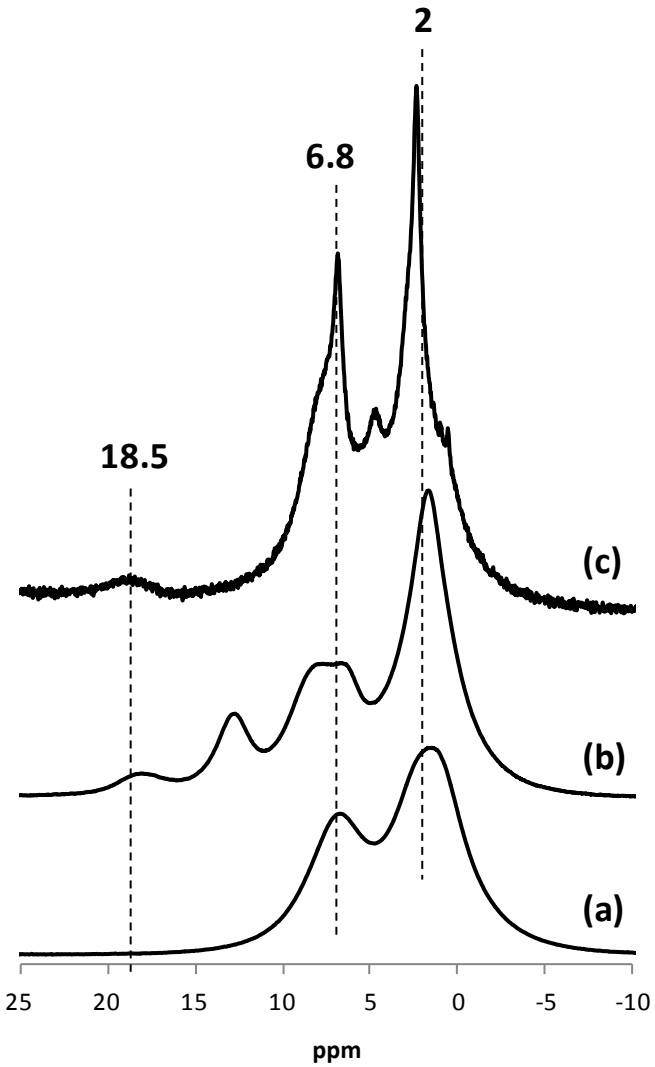

Figure 3: Height-normalized fluorescence emission spectra of DMAN aqueous solutions at different concentrations and as-prepared ITQ-51 solid, measured at different excitation wavelengths (270, 285, and 300 nm). The arrow indicates the second-order emission.

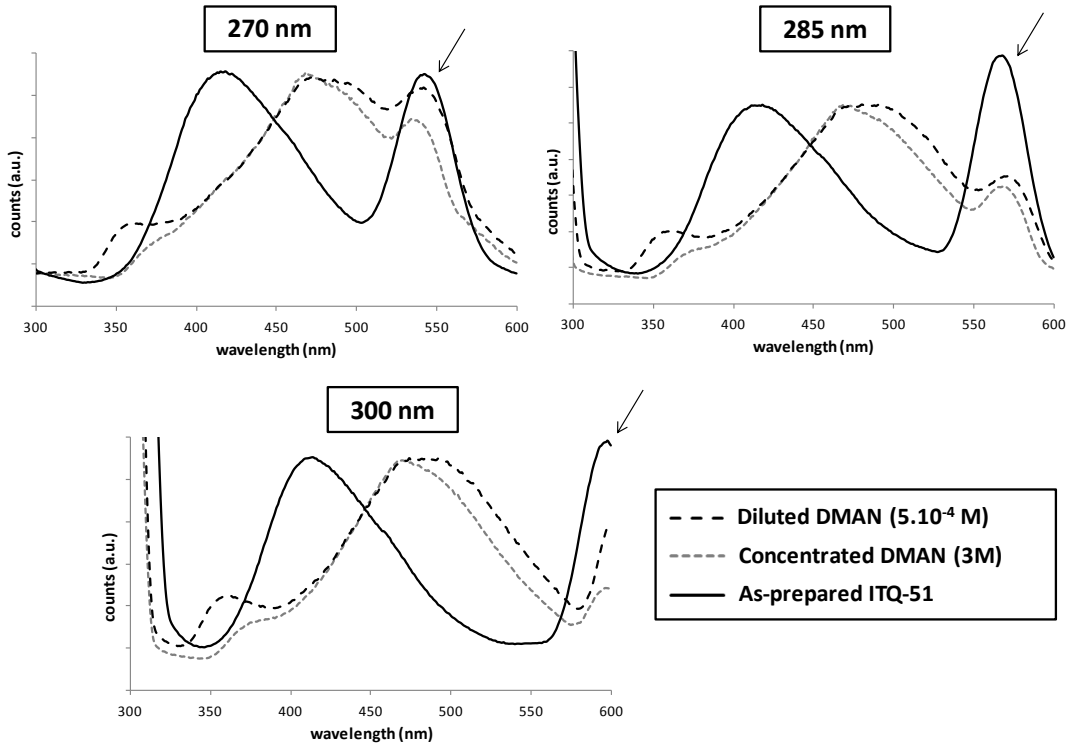

Figure 4: Observed (blue), calculated (red) and difference (black) PXRD profiles for the Rietveld refinement of the as-prepared ITQ-51 (λ = 1.5406 Å). The higher angle data has been scaled up (inset) to show the good fit between the observed and the calculated patterns.

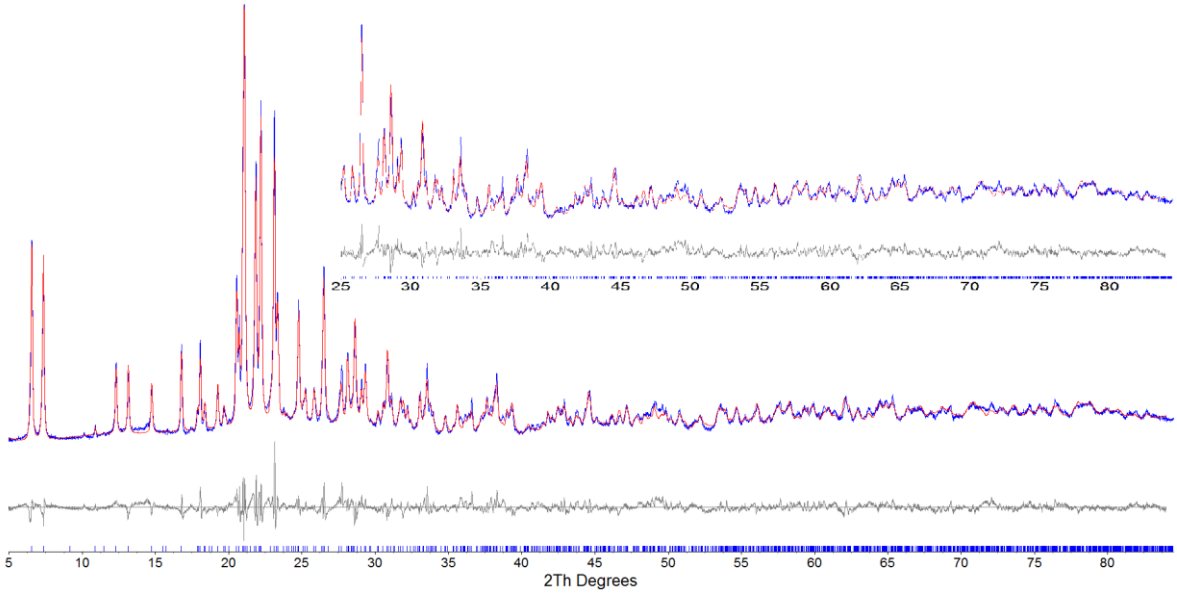

Figure 5: The structure of experimental as-prepared ITQ-51 zeolite viewed along [001] (a), and viewed along [010] (b). For clarity, the OSDAs in the channels on the edges of the unit cell were removed.

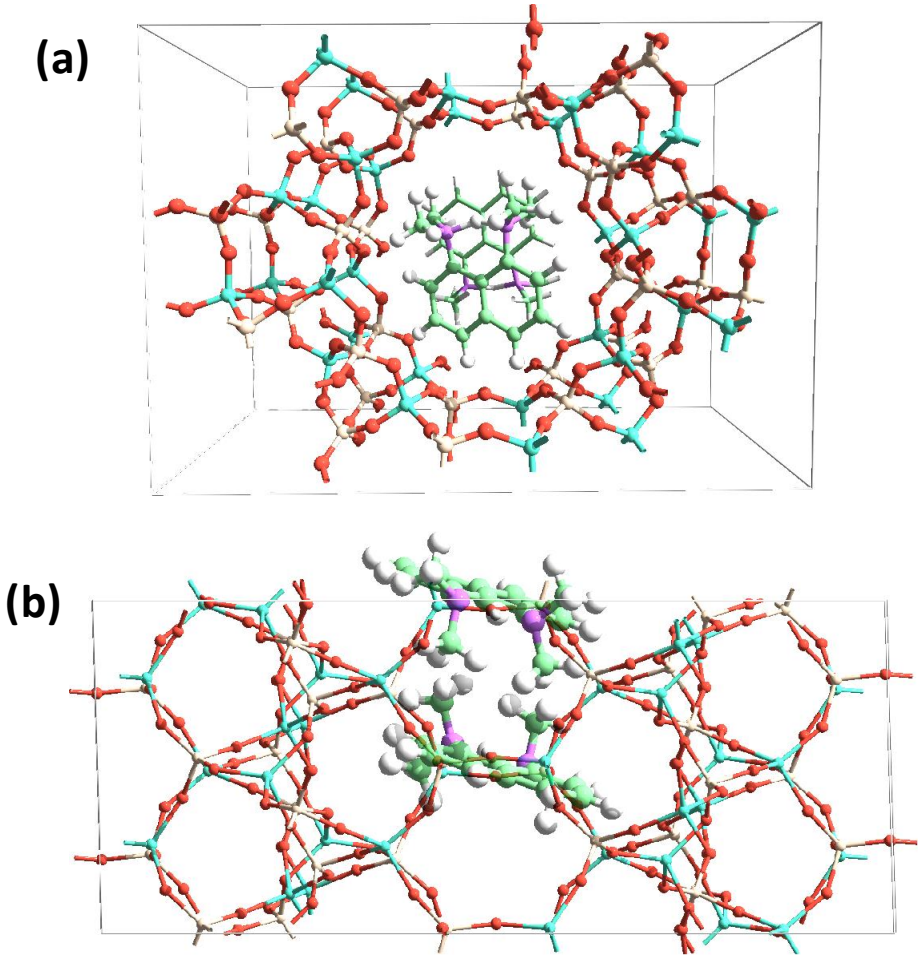

Figure 6: Views of the relative OSDA locations as calculated in the ITQ-51 zeolite. The distance between the OSDA molecules is 4.3 Å.

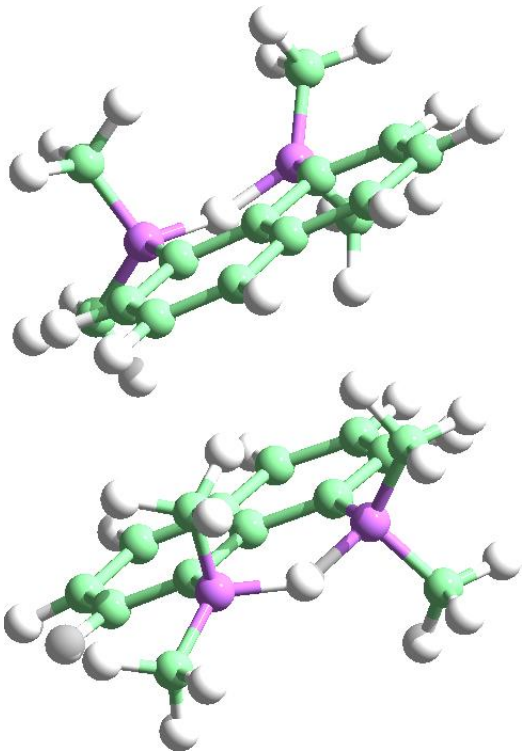

Supplementary Material

Figure S1: Solid ^{13}C MAS NMR of as-prepared ITQ-51 molecular sieve (top) and liquid ^{13}C NMR of proton sponge DMAN (bottom).

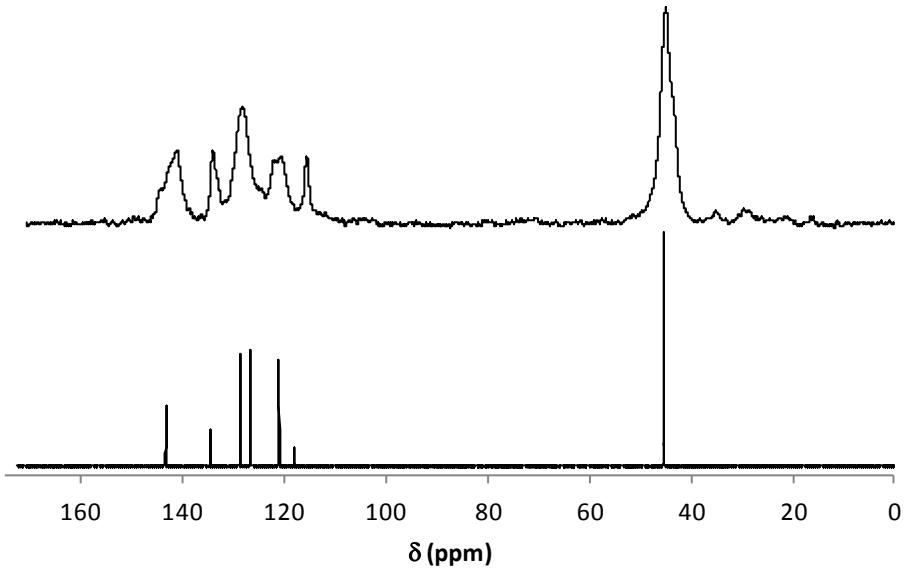

Figure S2: UV-Vis spectrum of DMAN in aqueous solution.

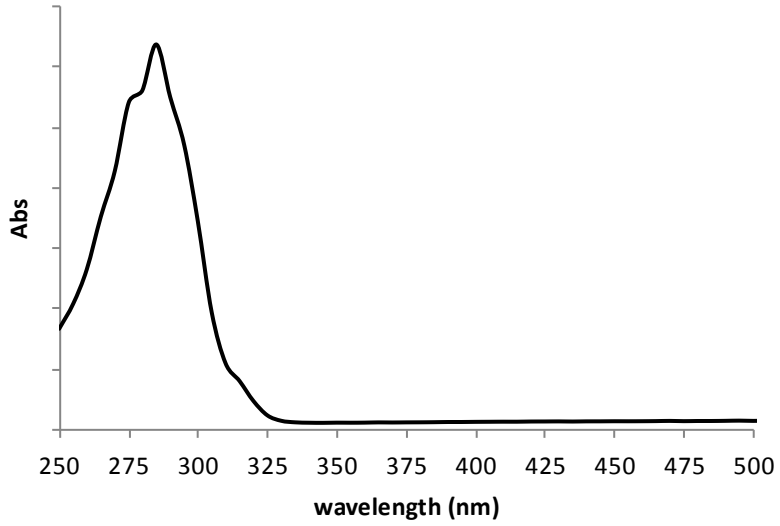

Figure S3: Liquid ^{1}H NMR spectra of an aqueous solution of DMAN at 5.10^{-4} M (a), at 3 M (b), and solid ^{1}H MAS NMR spectrum of the as-prepared ITQ-51 zeotype (c).

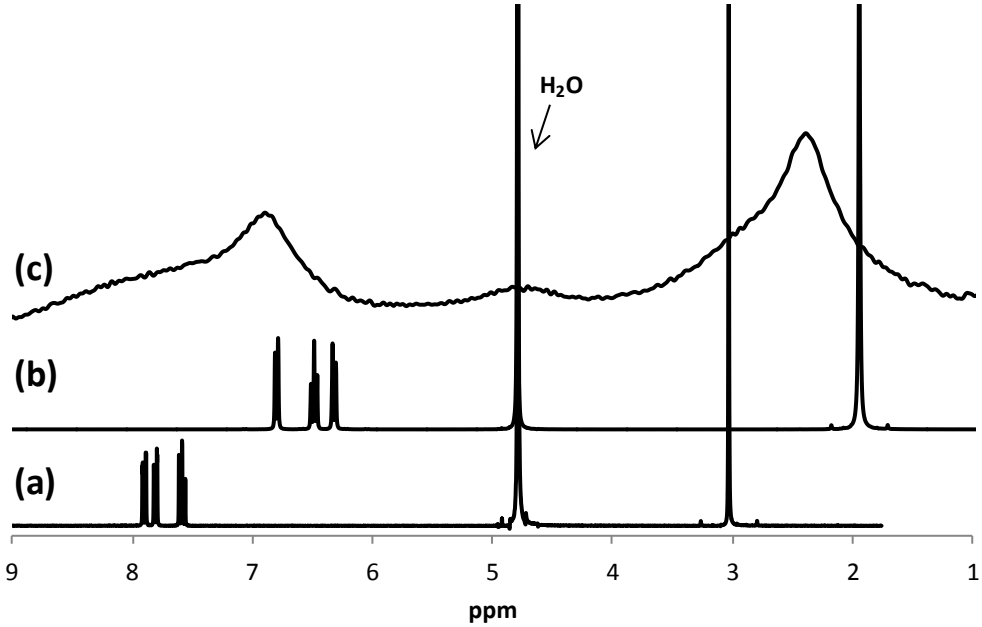

Figure S4: Views of the calculated unit cell of ITQ-51.

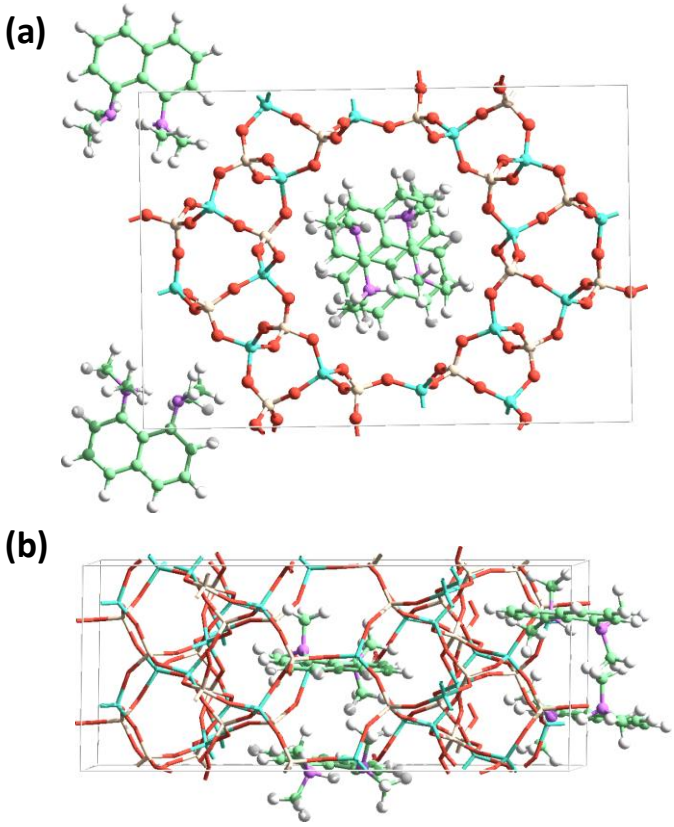

Table S1: Crystallographic data for Rietveld refinement of as-prepared ITQ-51.

Chemical formula	$(C_{14}N_2H_{18}H)_{0.5}Al_4P_4O_{16}$
Formula weight	2381.88
a	24.0445(11) Å
b	16.2542(6) Å
c	5.0485(2) Å
β	88.433(3)°
V	1972.32(14) $Å^3$
Z	4
Space group	$P2_1/n$ (no.14)
CuKα_1	1.5406 Å
No. of reflections	1380
No. of parameters	117
No. of restraints	384 T-O distances, rigid body for SDA and distance among the SDA and frameworks
R_p	0.0521
R_{wp}	0.0667
R_{exp}	0.0263
GOF	2.536
R_F	0.0281

Table S2: Comparison of experimental and calculated cell parameters of as-prepared ITQ-51.

Parameter	Calculated	Experimental	Difference (exp-calc)
a	23.61 Å	24.04 Å	+0.43 Å (1.8%)
b	16.25 Å	16.25 Å	+0.00 Å (0.0%)
c	4.95 Å	5.05 Å	+0.10 Å (2.0%)
α	90.0º	90.0º	
β	90.9º	88.433(3)°	
γ	90.0º	90.0º	
Volume	1897.67 $Å^3$	1972.32 $Å^3$	74.67 $Å^3$ (3.8%)
tilt	82º	74º	

Table S3: Stabilization energy (kJ/mol) of the OSDAs in the ITQ-51 zeotype. The values have been calculated for the optimum loading, which includes 4 OSDA molecules in a 1x1x2 unit cell of ITQ-51. With these values, a total stabilization energy of -342 kJ is obtained according to eq (3) [$\Delta E_{synthesis} = \Delta E_{frame} + E_{frame'-OSDA'} + \Delta E_{OSDA-OSDA} + \Delta E_{OSDA}$].

$\Delta E_{synthesis}$	ΔE_{frame}	$E_{frame'-OSDA'}$	$\Delta E_{OSDA-OSDA}$	ΔE_{OSDA}
-409	+80	-364	-145	+20

References

[1] (a) Lobo, R. F., Zones, S. I., & Davis, M. E. 1995 Structure-direction in zeolite synthesis. *J. Inclus. Phen. Mol. Rec*. 21, 47-78; (b) Moliner, M., Rey, F. & Corma, A. 2013 Towards the Rational Design of Efficient Organic Structure-Directing Agents for Zeolite Synthesis. *Angew. Chem. Int. Ed*. doi: 10.1002/anie.201304713**.**

[2] (a) Freyhardt, C. C., Tsapatsis, M., Lobo, R. F., Balkus, K. J., & Davis, M. E. 1996 A high-silica zeolite with a 14-tetrahedral-atom pore opening. *Nature.* 381, 295-298; (b) Wagner, P., Yoshikawa, M., Lovallo, M., Tsuji, K., Tsapatsis, M. & Davis, M. E. 1997 CIT-5: A high-silica zeolite with 14-ring pores. *Chem. Commun.* 2179-2180; (c) Burton, A. W., Elomari, S., Chen, C. Y., Medrud, R. C., Chan, I. Y., Bull, L. M., Kibby, C., Harris, T. V., Zones, S. I. & Vittoratos, E. S. 2003 SSZ-53 and SSZ-59: Two novel extra-large pore zeolites. *Chem. Eur. J.*, 9, 5737-5748.

[3](a) Corma, A., Díaz-Cabañas, M. J., Jiang, J., Afeworki, M., Dorset, D. L., Soled, S. L. & Strohmaier, K. G. 2010 Extra-large pore zeolite (ITQ-40) with the lowest framework density containing double four- and double three-rings. *Proc. Natl. Acad. Sci. U.S.A.* 107, 13997-14002; (b) Corma, A., Díaz-Cabañas, M. J., Rey, F., Nicolopoulus, S. & Boulahya, K. 2004 ITQ-15: The first ultralarge pore zeolite with a bi-directional pore system formed by intersecting 14- and 12-ring channels, and its catalytic implications. *Chem. Commun.* 1356-1357.

[4](a) Sun, J., Bonneau, C., Cantin, A., Corma, A., Diaz-Cabanas, M. J., Moliner, M., Zhang, D., Li, M. & Zou, X. 2009 The ITQ-37 mesoporous chiral zeolite. *Nature*. 458, 1154-1159; (b) Jiang, J., Jorda, J. L., Yu, J., Baumes, L. A., Mugnaioli, E., Diaz-Cabanas, M. J., Kolb, U. & Corma, A. 2011 Synthesis and Structure Determination of the Hierarchical Meso-Microporous Zeolite ITQ-43. *Science.* 333, 1131-1134.

[5] Kubota, Y., Helmkamp, M. M., Zones, S. I. & Davis, M. E. 1996 Properties of organic cations that lead to the structure-direction of high-silica molecular sieves. *Microporous Mater*. 6, 213-229.

[6] Corma, A., Rey, F., Rius, J., Sabater, M. J. & Valencia, S. 2004 Supramolecular self-assembled molecules as organic directing agent for synthesis of zeolites. *Nature.* 431, 287-290.

[7] (a) Gomez-Hortiguela, L., Lopez-Arbeloa, F., Cora, F. & Perez-Pariente, J. 2008 Supramolecular chemistry in the structure direction of microporous materials from aromatic structure-directing agents. *J. Am. Chem. Soc.* 130, 13274-13284; (b) Gomez-Hortiguela, L., Hamad, S., Lopez-Arbeloa, F., Pinar, A. B., Perez-Pariente, J. & Cora, F. 2009 Molecular Insights into the Self-Aggregation of Aromatic Molecules in the Synthesis of Nanoporous Aluminophosphates: A Multilevel Approach. *J. Am. Chem. Soc.* 131, 16509-16524.

[8]Martínez-Franco, R., Moliner, M., Yun, Y., Sun, J., Wan, W., Zou, X. & Corma, A. 2013 Synthesis of an extra-large molecular sieve using proton sponges as organic structure-directing agents. *Proc. Natl. Acad. Sci. U.S.A.* 110, 3749-3754.

[9] Staab, H. A. & Saupe, T. 1988 “Proton sponges” and the geometry of hydrogen bonds: Aromatic nitrogen bases with exceptional basicities. *Angew. Chem., Int. Ed*. 27, 865-879.

[10] Catlow, C. R. A. & Cormack, A. N. 1987 Computer modeling of silicates. *Int. Rev. Phys. Chem*. 6, 227-250.

[11] (a) Gale, J. D. 1997 GULP: a computer program for the symmetry-adapted simulation of solids. *J. Chem. Soc. Faraday Trans*. 93, 629-637; (b) Gale, J. D. & Rohl, A. L. 2003 The general utility lattice program (GULP). *Mol. Simul*. 29, 291-341.

[12] Kiselev, A. V., Lopatkin, A. A. & Shulga, A. A. 1985 Molecular statistical calculation of gas adsorption by silicalite. *Zeolites.* 5, 261-267.

[13] Sastre, G., Lewis, D. W. & Catlow, C. R. A. 1996 Structures and Stability of Silica Species in SAPO Molecular Sieves. *J. Phys. Chem.* 100, 6722-6730.

[14] Yanai, T., Tew, D. & Handy, N. 2004 A new hybrid exchange–correlation functional using the Coulomb-attenuating method (CAM-B3LYP). *Chem. Phys. Lett*. 393, 51-57.

[15] Tawada, Y., Tsuneda, T., Yanagisawa, S., Yanai, T. & Hirao, K. 2004 A long-range-corrected time-dependent density functional theory. *J. Chem. Phys*. 120, 8425-8433.
[16] Schaefer, A., Horn, H. & Ahlrichs, R. 1992 Fully optimized contracted gaussian basis sets for atoms Li to Kr. *J. Phys. Chem.* 97, 2571-2577.
[17] (a) Wozniak, K., He, H., Klinowski, J., Jones, W. & Barr, T. L. 1995 ESCA, Solid-state NMR, and X-ray Diffraction Monitor the Hydrogen Bonding in a Complex of 1,s-Bis(dimethy1amino)naphthalene with 1,ZDichloromaleic Acid. *J. Phys. Chem*. 99, 14667-14677; (b) Rodriguez, I., Sastre, G., Corma, A. & Iborra, S. 1999 Catalytic Activity of Proton Sponge: Application to Knoevenagel Condensation Reactions. *J. Catal.* 183, 14–23.
[18] (a) Wozniak, K., He, H., Klinowski, J., Barr & T. L., Milart, P. 1996 ESCA and solid-state NMR studies of ionic complexes of 1,8-bis(dimethylamino)naphthalene. *J. Phys. Chem*. 100, 11420-11426; (b) Wozniak, K., Krygowski, T. M., Pawlak, D., Kolodziejski, W. & Grech, E. 1997 Solid-state NMR and x-ray diffraction studies of ionic complex of 1,8-bis(dimethylamino)naphthalene (DMAN) with picrolonic acid. *J. Phys. Org. Chem*. 10, 814-824.
[19] Young, R. A. 1993 The Rietveld Method, IUCr Book Serials, Oxford Univ Press, New York.

Figure captions

Figure 1: Proton sponge 1,8-bis(dimethylamino)naphtalene [DMAN].

Figure 2: Solid ^{1}H MAS NMR spectra of DMAN (a), of the complex of DMAN with orthophosphoric acid (b), and as-prepared ITQ-51 molecular sieve (c).

Figure 3: Height-normalized fluorescence emission spectra of DMAN aqueous solutions at different concentrations and as-prepared ITQ-51 solid, measured at different excitation wavelengths (270, 285, and 300 nm). The arrow indicates the second-order emission.

Figure 4: Observed (blue), calculated (red) and difference (black) PXRD profiles for the Rietveld refinement of the as-prepared ITQ-51 (λ = 1.5406 Å). The higher angle data has been scaled up (inset) to show the good fit between the observed and the calculated patterns.

Figure 5: The structure of experimental as-prepared ITQ-51 zeolite viewed along [001] (a), and viewed along [010] (b). For clarity, the OSDAs in the channels on the edges of the unit cell were removed.

Figure 6: Views of the relative OSDA locations as calculated in the ITQ-51 zeolite. The distance between the OSDA molecules is 4.3 Å.

Short title

Extra-large zeotype synthesis by proton sponge assemblies